Submillisecond-response polymer network liquid crystals for mid-infrared applications

FANGWANG GOU,[1] RAN CHEN,[1,2] MINGGANG HU,[3] JUANLI LI,[3] JIAN LI,[3] ZHONGWEI AN,[2] AND SHIN-TSON WU[1,*]

[1]CREOL, The College of Optics and Photonics, University of Central Florida, Orlando, FL 32816, USA
[2]School of Materials Science and Engineering, Shaanxi Normal University, Xi'an 710119, China
[3]Xi'an Modern Chemistry Research Institute, Xi'an 710065, China
*swu@ucf.edu

Abstract: We formulated a high birefringence, large dielectric anisotropy, UV stable, and low absorption loss nematic liquid crystal mixture, named UCF-15, for mid-wave infrared (MWIR) applications. To achieve fast response time, we fabricated a polymer network liquid crystal (PNLC) using UCF-15 as host. At 40°C operating temperature, our PNLC shows 2π phase change at $\lambda = 4$ μm, submillisecond response time, and over 98% transmittance in the 3.8 to 5.1 μm region. Potential applications of this PNLC phase modulator for high speed laser beam steering, adaptive optics, and optical tweezer are foreseeable.

1. Introduction

Liquid crystal (LC) based spatial light modulators (SLMs) have found useful applications for laser beam steering [1–3], adaptive optics [4,5], adaptive lens [6], and optical tweezer [7]. However, to achieve a 2π phase change especially in the mid-wave infrared (MWIR) region, a relatively thick LC layer is required, which dramatically increases the response time. Furthermore, the LC absorption in the MWIR region originating from molecular vibrations and overtones could be strong, depending on the functional groups [8]. The absorbed light would raise the temperature locally, which in turn causes nonuniform phase profile and degrade the device performance. Therefore, developing a LC material with fast response time, low absorption loss, and low operating voltage for MWIR SLM is urgently needed.

To improve response time while keeping 2π phase change in the MWIR region, polymer network liquid crystal (PNLC) has been proposed [9,10]. By mixing the LC host with a small amount (4-6%) of monomer, polymer network with submicron domain size can be formed to provide strong anchoring energy, which helps shorten the response time significantly. However, a major tradeoff is increased operating voltage ($V_{2\pi}$). In order to reduce voltage, on the device side, we can increase the domain size by reducing the monomer concentration. On the material side, we can use a LC with large dielectric anisotropy ($1/\Delta\varepsilon$) because $V_{2\pi} \sim \sqrt{1/}$. Another approach is to reduce cell gap (d), which demands a high birefringence (Δn) LC host. To fulfill these requirements, fluorinated terphenyl compounds are promising candidates [10,11]. In addition, polar groups with strong dipole moment such as cyano (CN) helps to enhance $\Delta\varepsilon$ and Δn. To suppress the absorption loss in the MWIR region, one effective approach is to shift the absorption bands outside the spectral region of interest by choosing a proper polar group [12,13]. For example, replacing hydrogens in the alkyl chain and aromatic rings with heavier atoms, such as fluorine (F) or chlorine (Cl), will shift the vibration absorption band to longer wavelength. Furthermore, fluoro and chloro polar groups offer high resistivity, good UV stability, and modest dipole moment [14–16].

In this paper, we developed a nematic LC mixture with high Δn, large $\Delta\varepsilon$, and low absorption loss in the MWIR region. Using this mixture, we fabricated a PNLC sample with 2π phase change and submillisecond response time at $\lambda = 4$ μm and $T = 40$°C, which is a
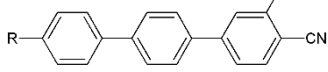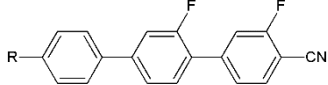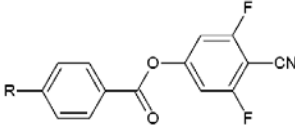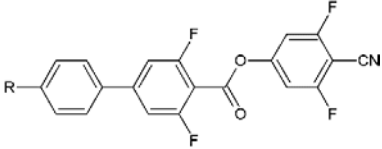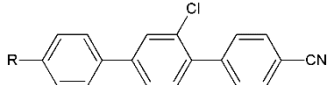
typical operating temperature for liquid-crystal-on-silicon (LCOS) devices due to the thermal effect from backplane driving circuits.

2. Experiment and results

2.1 LC mixture formulation

Fluorinated cyano-terphenyl LC compounds offer high Δn, large $\Delta\varepsilon$, and excellent UV stability, thus, they are good PNLC candidates for achieving fast response time [10]. However, these compounds have a relatively high melting point (T_m), which limits their applications. To lower the melting point, we formulated a eutectic mixture (called M1) with compounds 1 and 2 listed in Table 1. The terphenyl core extends the conjugation and increases birefringence. In compound 2, the interannular twisting and steric repulsion of molecules occur because of the two lateral fluoro substitutions at different rigid mesogenic unit, which helps to improve the solubility at low temperature and reduce the melting point. In order to boost $\Delta\varepsilon$ while keeping high Δn and good solubility, we doped 15.0 wt% of two fluorinated cyano-ester compounds 3 and 4 into M1 to form a new mixture M2. Two fluoro substitutions in the (3, 5) positions of a phenyl ring together with the terminal CN group in compounds 3 and 4 lead to a large $\Delta\varepsilon$, which helps to reduce the operating voltage. Since compound 3 has only two phenyl rings to contribute to molecular conjugation, its Δn is relatively low, but its solubility is good. In addition, the ester group in compounds 3 and 4 interrupts the molecular π–π interactions and helps to lower the melting point. As expected, the mixture M2 exhibits high Δn (0.31@ 633 nm) and large $\Delta\varepsilon$ (36) at room temperature. However, its melting point is about 20°C, which is still not low enough for practical applications.

Table 1. Chemical structures and weight of compounds employed.

Compound No.	Chemical structure	Weight (wt%)
1		76.5%
2		
3		13.5%
4		
5		10.0%

To further lower the melting point while keeping high Δn, large $\Delta\varepsilon$ and low absorption loss in the MWIR region, we applied the density functional theory computation [17] to select

an appropriate molecular structure (compound 5) as listed in Table 1. The calculation indicates that C–Cl bond is preferred in terms of absorption because its fundamental vibration bands occur in the 12.5–15.4 µm region, and the overtones are also outside the MWIR range. In addition, the chlorinated biphenyl ring has a twist angle of about 53.73°, which minimizes the π–π interaction to decrease the melting point. Besides, the large dipole moment (~6.95) of compound 5 helps to maintain large Δε. We mixed 10 wt% compound 5 with 90 wt% M2, and designated the final mixture as UCF-15. Remarkably, the melting point of UCF-15 drops to below −40°C (limited by our differential scanning calorimetry) due to super-cooling and its clearing point (T_c) is 150°C. The mixture was then stored in two refrigerators: one at 0°C and another at about −10°C. After 7 days, no crystallization was observed for the one stored at 0°C but the one at −10°C was precipitated. Therefore, the melting point of UCF-15 without super-cooling is estimated to be around −5°C.

2.2 Physical properties of LC host

In experiment, we measured the physical properties of UCF-15 including birefringence, absorption loss, dielectric anisotropy, and visco-elastic constant. The obtained results are summarized in Table 2. For practical applications, the actual operating temperature is about 35°C ~45°C due to the thermal effect of driving backplane [18]. Therefore, all the data listed here are intended for the operation at 40°C.

Table 2. Measured phase transition temperatures and physical properties of UCF-15 at T = 40°C and 1 kHz.

	Δn @ $\lambda = 4$ µm	$\Delta\varepsilon$	γ_1/K_{11} (ms/µm²)	E_a (meV)	T_m (°C)	T_c (°C)
UCF-15	0.248	30.4	56.72	477.54	−5	150

To measure birefringence in the visible and near-infrared region, we first injected UCF-15 mixture into a commercial 8-µm-thick homogenous cell with ITO (indium tin oxide) glass substrates. The cell was then mounted in a Linkam heating stage controlled by the temperature program (Linkam TMS94) to keep the testing temperature at 40°C. Birefringence was measured through the voltage-dependent transmittance (VT) of the homogenous LC sandwiched between two crossed linear polarizers. The probing light sources were a tunable Argon-ion laser (λ = 457 nm, 488 nm, and 514 nm), a He-Ne laser (λ = 633 nm) and two semiconductor lasers (λ = 1.06 µm and λ = 1.55 µm). A 1 kHz square-wave AC signal was applied to the LC cell. Birefringence at each wavelength was obtained from the phase retardation $\delta = 2\pi d\Delta n/\lambda$. To measure birefringence in the MWIR, the phase difference measurement technique [19] was used. We fabricated a homogenous LC cell with thickness of ~10.8 µm using two polyimide-coated sapphire substrates. The cell was sandwiched between two wire grid polarizers with the LC director oriented at 45° with respect to the transmission axis of polarizer. The transmission spectra when two polarizers are crossed ($I_\perp$) and paralleled ($I_{//}$) were measured by FTIR (Perkin Elmer Spectrum One FTIR Spectrometer) at 40°C. The birefringence was deduced by the recorded $I_\perp/I_{//}$. Results are included in Fig. 1(a), where dots are measured data and solid line is theoretical fitting with the single-band birefringence dispersion equation [20]:

$$\Delta n = G \frac{\lambda^2 \cdot \lambda^{*2}}{\lambda^2 - \lambda^{*2}}. \tag{1}$$

In Eq. (1), G is a proportionality constant and λ^* is the mean resonance wavelength. The obtained fitting values are G = 3.767 µm⁻² and λ^* = 0.255 µm. According to Fig. 1(a), as wavelength extends to MWIR region, birefringence decreases to a plateau and its value is about 20%~30% lower than that of visible region. In the vicinity of $\lambda \approx 3.4$ µm, birefringence fluctuates because of the resonance effect of the CH/CH₂/CH₃ vibration bands. While in the

off-resonance region, the experimental data agree well with the fitting using Eq. (1). At $\lambda = 4$ µm and $T = 40°C$, the measured birefringence is 0.248, which is very close to the extrapolated data (0.245). Such a high Δn enables a thin cell gap ($d \approx 16.2$ µm) to achieve 2π phase change, which in turn improves the transmittance and response time in the MWIR region. For a reflective SLM, such as LCOS, the cell gap can be reduced by 2x, i.e. 8.1 µm. As a result, the response time is improved by 4x, but the absorption loss remains the same.

To measure the transmittance at MWIR, we fabricated a LC cell with thickness of 18 µm using two bare sodium chloride (NaCl) substrates. The NaCl substrate is transparent from visible to 14 µm and its refractive index is about 1.52 in the MWIR, which is very close to that of the LC. In order to eliminate the light scattering of LC at nematic phase, we gently rubbed the inner surface of NaCl substrates so that the LC molecules can be homogeneously aligned. The result has been corrected to eliminate the reflection losses from the outer surfaces of the substrates. An absorption peak with narrow bandwidth occurs at $\lambda = 4.48$ µm due to the CN vibration. The baseline transmittance in the off-resonance region (3.8 µm ~5.1 µm) is over 98%.
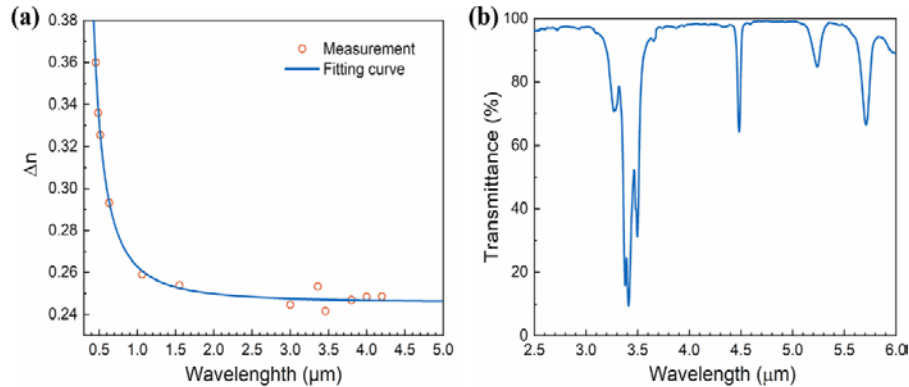

Fig. 1. (a) Birefringence dispersion of UCF-15 at $T = 40°C$: dots are measured data and solid line is fitting with Eq. (1). (b) Measured transmittance of UCF-15 in the MWIR region with cell gap $d = 18$ µm.

Next, we measured the temperature dependent birefringence because the intended operating temperature is 40°C. The testing temperature was increased from 22°C to 130°C and the results for $\lambda = 633$ nm are illustrated in Fig. 2(a). The dots represent measured data and solid line is fitting curve using Haller's semi-empirical equation [21]:

$$\Delta n = \Delta n_0 (1 - T / T_c)^\beta, \tag{2}$$

where Δn_0 is the extrapolated birefringence at $T = 0K$ and β is a material constant. Through fitting, we found $\Delta n_0 = 0.37$ and $\beta = 0.18$.

LC response time is linearly proportional to the visco-elastic coefficient (γ_1/K_{11}), which can be extracted by measuring the transient free relaxation time. Figure 2(b) plots the results (dots) and the fitting curve (solid line) with following equation [22]:

$$\frac{\gamma_1}{K_{11}} = A \cdot \frac{\exp(E_a / k_B T)}{(1 - T / T_c)^\beta}, \tag{3}$$

where A is a proportionality constant, k_B is the Boltzmann constant, E_a is the activation energy, and β is the material constant obtained from Eq. (2). As can be seen from Fig. 2(b), γ_1/K_{11} is highly dependent on the temperature. For a LC material, activation energy determines the decreasing rate of γ_1/K_{11} as temperature increases [23]. Through fitting, we found $E_a = 477.54$ meV and $A = 9.52 \times 10^{-7}$ ms/µm². At room temperature ($T = 22°C$), γ_1/K_{11}

= 170 ms/µm². As the temperature increases to 40°C, the visco-elastic coefficient drops dramatically to 57 ms/µm² while the birefringence only decreases slightly (Fig. 2(a)), which enables UCF-15 to be operated at elevated temperature to improve the response time and maintain adequate phase change simultaneously. However, the γ_1/K_{11} is still too large to achieve a fast response time for beam steering devices. For example, the estimated relaxation time is as slow as 420 ms if UCF-15 works in a reflective LCOS with $d = 8.5$ µm. Therefore, polymer network liquid crystal (PNLC) is a preferred choice for achieving fast response time.
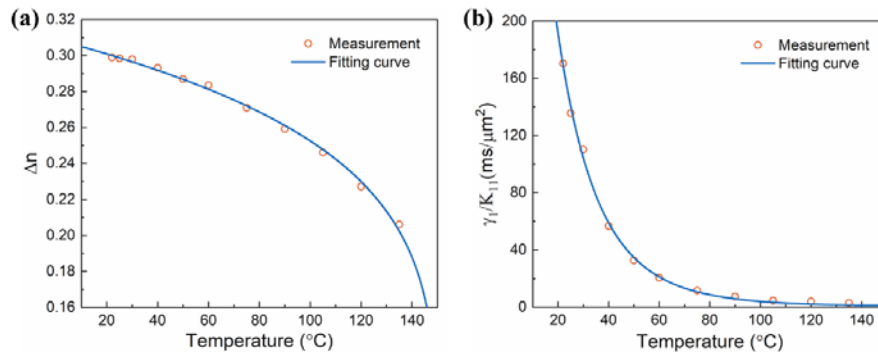

Fig. 2. (a) Birefringence and (b) visco-elastic coefficients of UCF-15 as a function of temperature. Dots are measured data and solid lines are fitting with Eq. (2) and Eq. (3), respectively. $\lambda = 633$ nm.

2.3 Polymer network liquid crystals

To fabricate PNLC, we first prepared precursor by adding 5.3 wt% mesogenic monomer RM257 (Merck) and 0.2 wt% photo-initiator Irgacure 819 to LC host UCF-15. Next, the precursor was filled into a 14.5-µm homogeneous LC cell with ITO glass substrates. The cell was operated in reflective mode to obtain 2π phase change at $\lambda = 4$ µm and to lower operating voltage. A 385-nm UV lamp was used to cure the sample at 25°C with UV intensity of ~200 mW/cm² for 1 hour. The terphenyl core and polar groups (-F, -Cl and -CN) are UV stable, which makes UCF-15 a good PNLC host. For simplicity, we fabricated PNLC device using ITO glass substrates and measured the electro-optical properties of PNLC samples at $\lambda = 1.55$ µm because the ITO glass substrates are not transparent at $\lambda = 4$ µm. The experimental setup is the same as that for measuring the VT curves. According to the dispersion curve shown in Fig. 1(a), the LC birefringence is insensitive to the wavelength in the IR region. Therefore, based on equation $\delta = 2\pi d\Delta n/\lambda$, we converted the voltage-dependent phase curve from $\lambda = 1.55$ µm to $\lambda = 4$ µm. Figure 3 shows the results of PNLC sample with 5.3 wt% RM257. At $V = 120$ V$_{rms}$, 2π phase change can be achieved for reflective mode at $T = 40$°C.
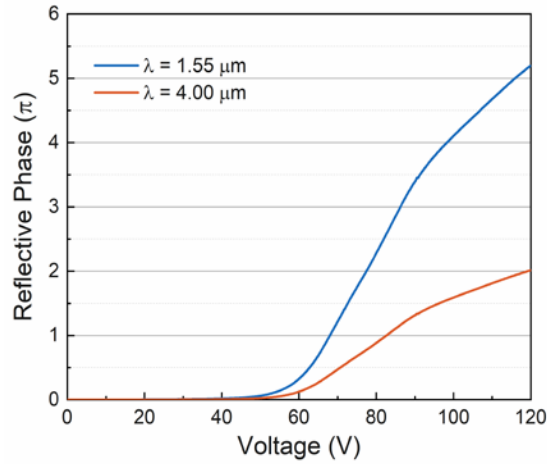
Fig. 3. Voltage-dependent phase change of our PNLC device in reflective mode at $\lambda = 1.55$ μm and $\lambda = 4$ μm. Cell gap d = 14.5 μm, and operating temperature $T = 40°C$.

To study relaxation time, we instantaneously removed the applied voltage ($120V_{rms}$) and recorded the transient phase change. The measured phase relaxation time is calculated between 90% and 10% phase change. Results at different operating temperatures are plotted in Fig. 4(a). As Eq. (3) shows, the visco-elastic coefficient decreases as temperature increases, which contributes to a faster response time. At $T = 40°C$, the measured relaxation time is $\tau = 0.85$ ms, which is valuable for MWIR laser beam steering. Another reason for such a fast response time results from suppressed double relaxation [24] at elevated temperature. For a polymer-stabilized system, usually the relaxation process cannot be well fitted by a single exponential decay because of the sophisticated interaction between polymer network and LC molecules, as can be seen from Fig. 4(b). Two relaxation processes are often involved: 1) the relaxation of submicron LC domains, and 2) electrostriction effect of the polymer networks [25]. The former process is much faster than the latter. To quantitatively analyze the double relaxation, we fit the measured phase change by the following equation:

$$\delta(t) = A \times e^{-t/\tau_1} + B \times e^{-t/\tau_2}, \tag{4}$$

where the first term and the second term represent the fast relaxation and the slow relaxation, respectively, and [A, B] and [τ_1, τ_2] are the corresponding weights and time constants. The degree of single relaxation can be quantified as the ratio $A/(A + B)$. If the ratio reaches one (i.e. $B = 0$), it stands for single relaxation due to the fact that second term is vanished. For a stronger double relaxation case, B becomes larger so that $A/(A + B)$ is decreased. In our fitting, the ratio is 90% and the time constants are $\tau_1 = 0.78$ ms and $\tau_2 = 24.80$ ms at $T = 22°C$. In contrast, at $T = 40°C$, the ratio increases to 95% and the time constants are $\tau_1 = 0.28$ ms and $\tau_2 = 14.35$ ms, indicating a weaker double relaxation.
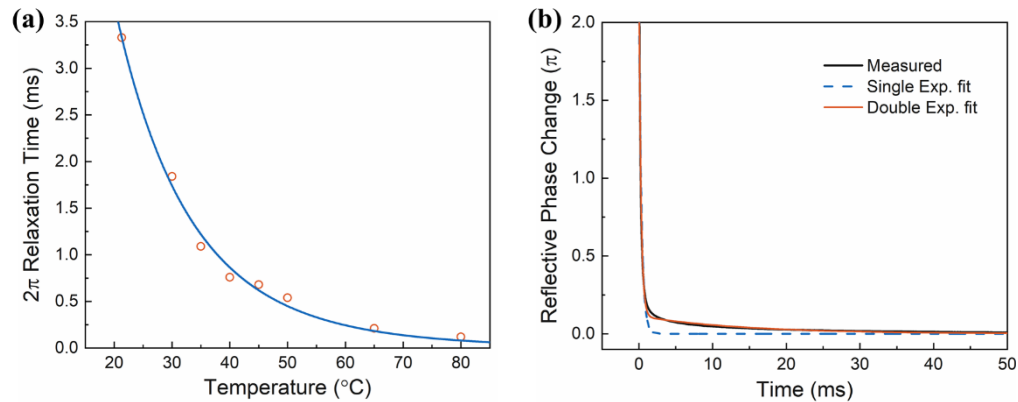
Fig. 4. (a) Temperature dependent relaxation time for 2π phase change of our PNLC device. (b) The transient relaxation process of the PNLC sample at $T = 40°C$ fitted with single (dashed blue line) and double (solid red line) relaxation curves.

For practical applications, light scattering loss is undesirable. To analyze the scattering, we plot the measured transmittance of PNLC sample at $V = 0$, 60 and 120 V_{rms} in Fig. 5. The transmittance is normalized to a sample cell filled with pure nematic LC host UCF-15. The oscillation is due to Fabry–Pérot interference from ITO glass substrates. As Fig. 5 depicts, in the voltage-off state ($V = 0$), PNLC sample is highly transparent because the LC directors are aligned well by the surface treatment. As the voltage increases, the LC molecules constrained by polymer network start to form multi-domains, which scatter light if the domain sizes are comparable to the wavelength [26]. As the voltage increases, scattering becomes stronger, especially in the short-wavelength infrared region. However, in the MWIR, the scattering is negligible because the wavelength is much larger than the domain size.
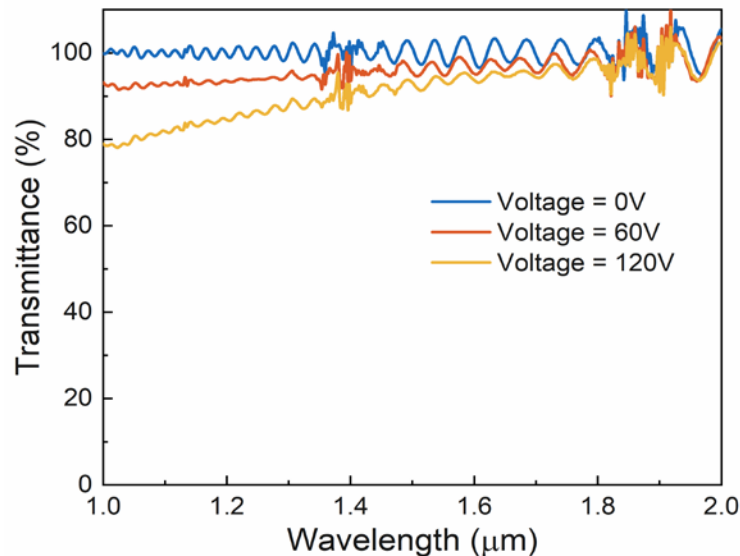

Fig. 5. Measured transmission spectra of PNLC sample at $V = 0$, 60 and 120 V_{rms}. Transmittance was normalized to the cell filled with pure nematic host UCF-15.

In order to balance the operating voltage and response time, we can modify the domain size of PNLC devices by controlling the monomer concentration and curing temperature. Table 3 lists the $V_{2\pi}$ and relaxation times for five PNLC samples at $\lambda = 4$ μm. As the monomer concentration increases from 5 wt% to 5.5 wt% while curing temperature keeps at 25°C, $V_{2\pi}$

increases but relaxation time decreases due to the smaller domain size. On the other hand, the domain size can be reduced by decreasing the curing temperature from 25°C to 10°C, while keeping the monomer concentration at 5 wt%. To obtain submillisecond relaxation time and reasonable operating voltage, we choose PNLC sample with 5.3 wt% monomer and curing temperature at 25°C.

Table 3. Operating voltage and relaxation time of PNLCs at λ = 4 µm and T = 40°C.

Sample	RM257 (wt%)	Curing T (°C)	$V_{2\pi}$ (V)	τ (ms)
1	5.0	25	97.6	1.91
2	5.3	25	119.4	0.85
3	5.5	25	>120	0.67
4	5.0	15	103.6	1.38
5	5.0	10	111.8	1.18

3. Conclusion

We have formulated a new liquid crystal mixture for phase modulation in the MWIR region. The mixture exhibits a broad nematic range, low absorption loss, high birefringence (Δn = 0.248 at 4 µm) and large dielectric anisotropy ($\Delta\varepsilon$ = 30.4) at intended operating temperature T = 40°C. When employed in a polymer network liquid crystal device, we can achieve submillisecond response time for 2π phase change at λ = 4 µm. This device is attractive for the applications in mid-infrared spatial light modulators. For practical applications, the ITO-glass can be replaced by a thin germanium substrate, which is both transparent and conductive in the IR region.

Funding

Acknowledgments

References

1. D. P. Resler, D. S. Hobbs, R. C. Sharp, L. J. Friedman, and T. A. Dorschner, "High-efficiency liquid-crystal optical phased-array beam steering," Opt. Lett. **21**(9), 689–691 (1996).
2. P. F. McManamon, P. J. Bos, M. J. Escuti, J. Heikenfeld, S. Serati, H. Xie, and E. A. Watson, "A review of phased array steering for narrow-band electrooptical systems," Proc. IEEE **97**(6), 1078–1096 (2009).
3. F. Gou, F. Peng, Q. Ru, Y. H. Lee, H. Chen, Z. He, T. Zhan, K. L. Vodopyanov, and S. T. Wu, "Mid-wave infrared beam steering based on high-efficiency liquid crystal diffractive waveplates," Opt. Express **25**(19), 22404–22410 (2017).
4. C. Li, M. Xia, Q. Mu, B. Jiang, L. Xuan, and Z. Cao, "High-precision open-loop adaptive optics system based on LC-SLM," Opt. Express **17**(13), 10774–10781 (2009).
5. S. Quirin, D. S. Peterka, and R. Yuste, "Instantaneous three-dimensional sensing using spatial light modulator illumination with extended depth of field imaging," Opt. Express **21**(13), 16007–16021 (2013).
6. H. Ren and S. T. Wu, *Introduction to Adaptive Lenses* (Wiley, 2012).
7. H. Kim, W. Lee, H. G. Lee, H. Jo, Y. Song, and J. Ahn, "In situ single-atom array synthesis using dynamic holographic optical tweezers," Nat. Commun. **7**, 13317 (2016).
8. S. T. Wu, "Absorption measurements of liquid crystals in the ultraviolet, visible, and infrared," J. Appl. Phys. **84**(8), 4462–4465 (1998).
9. J. Sun and S. T. Wu, "Recent advances in polymer network liquid crystal spatial light modulators," J. Polym. Sci. **52**(3), 183–192 (2014).
10. F. Peng, H. Chen, S. Tripathi, R. J. Twieg, and S. T. Wu, "Fast-response infrared phase modulator based on polymer network liquid crystal," Opt. Mater. Express **5**(2), 265–273 (2015).
11. M. Schadt, "Liquid crystal materials and liquid crystal displays," Annu. Rev. Mater. Sci. **27**(1), 305–379 (1997).
12. Y. Chen, H. Xianyu, J. Sun, P. Kula, R. Dabrowski, S. Tripathi, R. J. Twieg, and S.-T. Wu, "Low absorption liquid crystals for mid-wave infrared applications," Opt. Express **19**(11), 10843–10848 (2011).

13. F. Peng, Y. Chen, S.-T. Wu, S. Tripathi, and R. J. Twieg, "Low loss liquid crystals for infrared applications," Liq. Cryst. **41**(11), 1545–1552 (2014).
14. S. T. Wu, D. Coates, and E. Bartmann, "Physical properties of chlorinated liquid crystals," Liq. Cryst. **10**(5), 635–646 (1991).
15. M. Schadt, "Nematic liquid crystals and twisted-nematic LCDs," Liq. Cryst. **45**(5–6), 646–652 (2015).
16. M. Hird, "Fluorinated liquid crystals--properties and applications," Chem. Soc. Rev. **36**(12), 2070–2095 (2007).
17. P. Hohenberg and W. Kohn, "Inhomogeneous electron gas," Phys. Rev. **136**(3B), B864–B871 (1964).
18. M. S. Brennesholtz, "New-technology light sources for projection displays," SID Int. Symp. Digest Tech. Papers **39**(1), 858–861 (2008).
19. S. T. Wu, U. Efron, and L. D. Hess, "Infrared birefringence of liquid crystals," Appl. Phys. Lett. **44**(11), 1033–1035 (1984).
20. S. T. Wu, "Birefringence dispersions of liquid crystals," Phys. Rev. A Gen. Phys. **33**(2), 1270–1274 (1986).
21. I. Haller, "Thermodynamic and static properties of liquid crystals," Prog. Solid State Chem. **10**(2), 103–118 (1975).
22. S. T. Wu and C. S. Wu, "Rotational viscosity of nematic liquid crystals A critical examination of existing models," Liq. Cryst. **8**(2), 171–182 (1990).
23. H. Chen, M. Hu, F. Peng, J. Li, Z. An, and S. T. Wu, "Ultra-low viscosity liquid crystals," Opt. Mater. Express **5**(3), 655–660 (2015).
24. Y. H. Lee, F. Gou, F. Peng, and S. T. Wu, "Hysteresis-free and submillisecond-response polymer network liquid crystal," Opt. Express **24**(13), 14793–14800 (2016).
25. D. Xu, J. Yan, J. Yuan, F. Peng, Y. Chen, and S. T. Wu, "Electro-optic response of polymer-stabilized blue phase liquid crystals," Appl. Phys. Lett. **105**(1), 011119 (2014).
26. J. Sun, Y. Chen, and S. T. Wu, "Submillisecond-response and scattering-free infrared liquid crystal phase modulators," Opt. Express **20**(18), 20124–20129 (2012).